PCCP

ROYAL SOCIETY OF CHEMISTRY

PAPER

View Article Online
View Journal | View Issue

Cite this: *Phys. Chem. Chem. Phys.*, 2025, **27**, 14342

Deep-blue thermally activated delayed fluorescence of a CF3-substituted carbene–metal–amide complex†

Alexander C. Brannan,[a] Nguyen Le Phuoc,[b] Mikko Linnolahti *[b] and Alexander S. Romanov*[a]

Received 2nd March 2025,
Accepted 10th June 2025

DOI: 10.1039/d5cp00824g

rsc.li/pccp

A gold-based carbene–metal–amides (CMA) complex, **BICAuBGCF3**, with a 2-(trifluoromethyl)-benzoguanidine amide (**L**) ligand was prepared in good yields and characterized. The CF_3-substituted amide donor ligand resulted in a 0.27 eV stabilization of the highest occupied molecular orbital (HOMO) and a wide energy gap of 2.97 eV. In fluid media, the complex experiences dynamic behavior between two isomeric forms, which reduces the blue luminescence quantum yield to 43%. In the solid state, the complex shows bright deep-blue thermally activated delayed fluorescence at 432 nm with 60% luminescence quantum yield owing to a small singlet triplet energy gap (ΔE_{ST}) down to 54 meV. Radiative rates (k_r) were calculated to be up to 1.4×10^6 s^{-1} in amorphous polystyrene media, demonstrating the **BICAuBGCF3** complex as a p,romising material for optoelectronic applications.

Introduction

Bright and stable thermally activated delayed fluorescence (TADF) luminophores are highly sought after by the academic community and industry for optoelectronic applications, particularly as organic light-emitting diodes (OLEDs), photovoltaics and sensors.[1–3] This is because of their ability to harvest singlet and triplet excitons *via* reverse intersystem crossing (rISC) from the triplet (T_1) state to the singlet state (S_1).[4–9] Among the most high-performance TADF materials, carbene–metal–amide (CMA) materials have emerged as a promising class of organometallic TADF materials owing to their facile synthesis and spectacular performance in OLED devices.[10–12] Their common molecular design is based on a d^{10}-coinage metal (Cu, Ag or Au) with a near-linear arrangement of a π-donor amide and a π-acceptor carbene ligand in trans-position to each other. Various CMA materials have demonstrated luminescence across the whole visible spectrum with submicrosecond emission lifetimes and near unity photoluminescence quantum yields (PLQYs).[13–16]

Several orientations are possible because of the conformational flexibility of the donor and acceptor ligands of CMAs: fully-twisted, co-planar, tilted and twisted/tilted CMAs. Romanov *et al.* demonstrated that twisted and tilted geometry can achieve the highest radiative rates among CMAs with a similar molecular design.[17] Such conformational flexibility between carbene and amide moieties enables the control of the frontier orbital overlap integral (S_{HO}) between the highest occupied molecular orbital (HOMO), located on the amide donor ligand, and the lowest unoccupied molecular orbital (LUMO), located over the M-carbene bond. High-performance CMA materials possess charge transfer (CT) characteristics for the first singlet (S_1) and triplet (T_1) excited states. Recent studies have highlighted the importance of the molecular design principle minimising the frontier orbital overlap integral to reduce the energy difference between ^{1}CT and ^{3}CT excited states (ΔE_{ST}) and accelerate the radiative rates to above 10^6 s^{-1}.[18,19]

Recent works on CMA materials have highlighted the role of the energy difference between locally excited triplet (^{3}LE) and CT emissive states in CMA materials ($\Delta E_{(CT-3LE)}$),[20] where increasing the energy of the ^{3}LE state relative to the manifold of CT states enables near unity photoluminescence quantum yields (PLQYs) and high radiative rates of TADF.[21] CMA compounds are known for their high ground and excited state dipole moments, where emission energies are sensitive to their molecular environment; for example, this has allowed the "tuning" of electroluminescence from green to sky-blue using a suitable host media.[18b,20] Efficient blue emission from CMA complexes can be achieved by attaching electron-withdrawing

[a] *Department of Chemistry, The University of Manchester, Oxford Rd., Manchester, M13 9PL, UK. E-mail: alexander.romanov@manchester.ac.uk*
[b] *Department of Chemistry and Sustainable Technology, University of Eastern Finland, Joensuu Campus, FI-80101 Joensuu, Finland. E-mail: mikko.linnolahti@uef.fi*

† Electronic supplementary information (ESI) available. CCDC 2427966. For ESI and crystallographic data in CIF or other electronic format see DOI: https://doi.org/10.1039/d5cp00824g

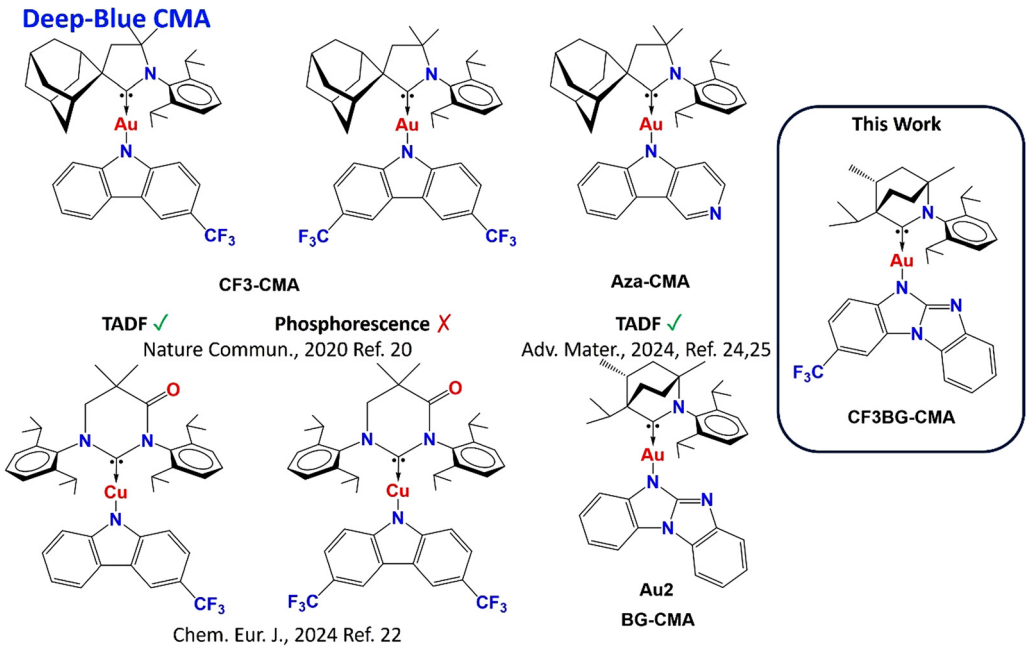

Scheme 1 Molecular structures of blue light-emitting CMA complexes.

CF_3 groups to the amide moiety to stabilize the HOMO energy and widen the energy gap (Scheme 1). This strategy achieved deep blue emission TADF for mono-CF_3-substituted CMA complexes; however, di-CF_3 substituted CMA complexes resulted in long-lived phosphorescent emission from the locally excited state of the carbazolide ligand, ^{3}LE(Cz).[20–22] Such CF_3-substituted CMA complexes appeared highly suitable for the fabrication of the energy transfer OLEDs.[23]

Recently, it was found that the energy of the ^{3}LE state can be increased for aza-CMA materials (Scheme 1), enabling faster and more efficient deep-blue TADF emission.[24] Electron-withdrawing aza-nitrogen substitution in *para*-position to the amide-N atom[24] have been further extended towards BG-CMA materials (Scheme 1).[25] The use of the benzoguanidine (BG) ligand with multiple aza-N atom substitutions in the donor ligand enabled the formation of champion BG-CMA materials exhibiting deep-blue TADF luminescence with high radiative rates of up to 4.69×10^6 s^{-1} due to a $\Delta E_{(CT-3LE)}$ of up to −0.5 eV and a reduced HOMO/LUMO overlap integral ($S_{H/L}$ = 0.25).[25] This outstanding photophysical behaviour motivated the team to build on the synergy between the two molecular design strategies for deep-blue CMA materials (Scheme 1). Herein, we investigated the first example of a CMA material containing an electron-withdrawing CF_3 moiety in a BG-donor ligand to demonstrate deep-blue TADF and reveal the structure–property relationship.

Results and discussion

A carbene–metal–amide (CMA) complex, **BICAuBGCF3**, was prepared by reacting the halide complex BiCAACAuCl with 2-(trifluoromethyl)-5*H*-benzo[*d*]benzo[4,5]imidazo[1,2-*a*]imidazole (**BGCF3**) in the presence of the KO^{t}Bu base in THF following our previously published protocol in high yield. The complex was found to be stable in air for several months.[25] This gold-based complex was characterized using ^{1}H, ^{19}F and ^{13}C{^{1}H} NMR spectroscopy (ESI†) and high-resolution mass spectrometry (HRMS). The product demonstrated high solubility in aromatic solvents (toluene, chlorobenzene, and 1,2-difluorobenzene), THF, and dichloromethane but was only sparingly soluble in hexane. On first inspection, the ^{1}H NMR spectrum of **BICAuBGCF3** appeared complicated with more signals than expected in the aryl region. A more detailed analysis revealed that signals in the 5.9–8.0 ppm region appeared in a set of two, with an integration ratio of 0.6 : 0.4 per assigned proton, while the number of upfield-shifted signals appear as expected for the complex, with an integration of 1 per assigned proton. This phenomenon was also observed in ^{19}F spectra, with two peaks appearing at −59.50 and −59.88 ppm, with a concurrent integration ratio of 0.6 : 0.4. The complementary integration between the down- and upfield-shifted protons suggests dynamic behavior in the solution of the complex, which is associated with the two possible isomers of the unsymmetrically substituted **BGCF3** ligand (Fig. 1). The ligand has two available N-binding sites, which result in two possible regioisomers: **A** and **B** (Fig. 1).

A series of varied-temperature NMR experiments were performed for the title complex in acetone-d_6 (at 50 °C) or upon cooling DCM-d_2 solution to −40 °C (Fig. S3 and S4, ESI†). However, no change was observed in the NMR spectra; for instance, the signals shifted by the same degree on cooling for each set, but the integration ratio of 0.6 : 0.4 was maintained. To further verify this, we isolated the single crystals of the title

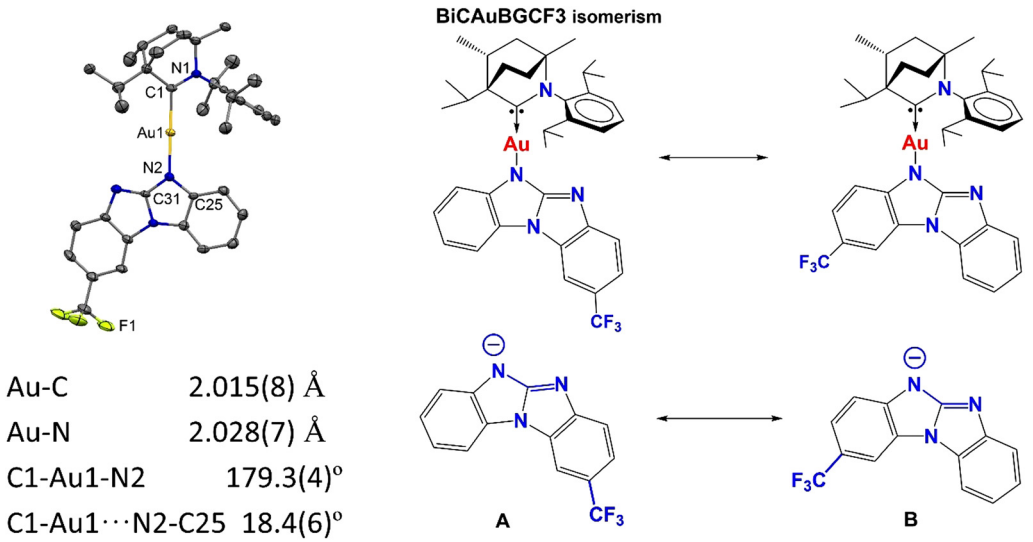

Fig. 1 Molecular and crystal structures of the carbene metal amide **BICAuBGCF3** (left) with key structural parameters. Ellipsoids are shown at 50% probability with hydrogen atoms omitted for clarity. Molecular structure of the two possible isomers (right).

complex with confirmed **A** geometry (Fig. 1) and dissolved them in DCM-d^2 again to run ^{1}H NMR spectra from the single crystals to confirm the presence of a single isomer. However, the NMR spectra demonstrated two sets of peaks with an integration ratio of 0.6 : 0.4, confirming the presence of isomerism in the fluid media. Our previous works demonstrated fluxional behaviour in the solution for copper-based CMA complexes with formamidinato and guanidinato ligands, where the (CAAC)Cu-fragment experienced a dynamic exchange between the two N-binding sites of the amido ligand.[26] Interestingly, BG-CMA complexes with the methoxy-substituted benzoguanidinato ligand have been reported as a single isomer, which is likely associated with the electron-donating nature of the methoxy substituent preferentially stabilising one isomeric form, **A**. The theoretically calculated energy difference between the two isomers **A** and **B** is 2.55 kJ mol^{-1}, where isomer **A** is energetically more favourable than isomer **B**.

The molecular structure of **BICAuBGCF3** was confirmed using single crystal X-ray diffraction, as shown in Fig. 1. We checked multiple single crystals and found only a single isomer **A**. The gold complex shows a linear two-coordinate geometry around the central gold atom with the C–Au–N angle at nearly 180°. The torsion angle between BIC carbene (N1–C1) and amide ligands (N2–C25) is 18.4(6)°, which is similar to that of complex **Au2**. The Au–N bond length is the same as that for the unsubstituted complex **Au2**, while the Au–C bond length is approximately 0.04 Å longer for **BICAuBGCF3** than that for **Au2**. This structural difference results in a 0.04-Å larger separation (C1···N2 distance) between donor and acceptor ligands for **BICAuBGCF3**, thus impacting its photophysical properties, *vide infra*.

Electrochemical properties

The redox behaviour of the title gold complex was analysed in THF solution using [^{n}Bu$_4$N]PF$_6$ as the supporting electrolyte

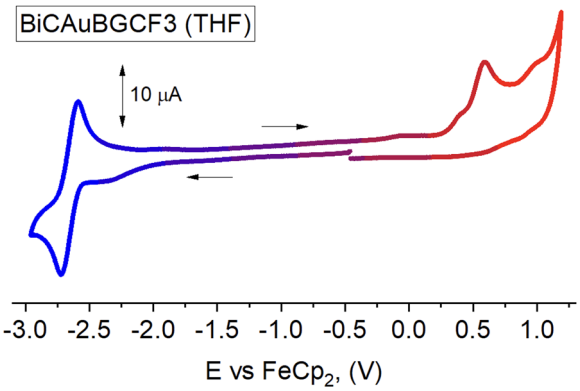

Fig. 2 Full-range cyclic voltammogram for the gold complex **BICAuBGCF3**.

(Fig. 2); the electrochemical data are summarised in Table 1. The **BICAuBGCF3** complex shows a quasi-reversible reduction process at −2.66 V, which is close to that of the analogous unsubstituted **Au2** complex[25a] (−2.78 V). This results in a 0.1-eV more stabilised LUMO energy level for the title complex (−2.83 eV) compared with **Au2** (−2.69 eV). The **BICAuBGCF3** complex shows an irreversible oxidation process at +0.59 V, which is 0.27 V anodically shifted compared with the analogous **Au2** complex (Table 1). This suggests that the electron-withdrawing CF$_3$ group stabilises the HOMO energy level for the title complex (−5.8 eV) compared with **Au2** (−5.53 eV), similar to the reported CF3–CMA complexes (Scheme 1).[20] Overall, the CF3 substituent results in a wide energy gap of 0.14 eV for the title complex, thus implying blue-shifted luminescent properties, *vide infra*.

Photophysical properties and theoretical calculations

The UV-vis absorption spectra for **BICAuBGCF3** were measured in cyclohexane, toluene, THF and dichloromethane solvents (Fig. 3). The complex shows high energy absorption bands in

Table 1 Formal electrode potentials (peak position E_p for irreversible and $E_{1/2}$ for quasi-reversible processes (*), *V, vs.* $FeCp_2$), onset potentials (*E, V, vs.* $FeCp_2$), peak-to-peak separation in parentheses for quasi-reversible processes (ΔE_p in mV), E_{HOMO}/E_{LUMO} (eV) and band gap values (ΔE, eV) for the investigated **BICAuBGCF3** complex and **BICAuBG** (**Au2**)[25a] analogue[a]

	Reduction			Oxidation				
	E_{1st}	$E_{onset\ red}$	E_{LUMO}, eV	E_{1st}	$E_{onset\ ox}$	E_{2nd}	E_{HOMO}, eV	ΔE, eV
BiCAuBG[25a]	−2.78 (161)	−2.70	−2.69	0.28	0.14	—	−5.53	2.83
BiCAuBGCF3[b]	−2.66 (130)	−2.56	−2.83	0.59	0.41	1.00	−5.80	2.97

[a] In THF solution, recorded using a glassy carbon electrode, concentration = 1.4 mM, supporting electrolyte [^{n}Bu$_4$N][PF$_6$] (0.13 M), measured at 0.1 V s^{-1}. [b] In THF solution, recorded using a glassy carbon electrode, concentration = 1.4 mM, supporting electrolyte [^{n}Bu$_4$N][PF$_6$] (0.13 M), measured at 0.1 V s^{-1}. $E_{HOMO} = -(E_{onset\ ox\ Fc/Fc+} + 5.39)$ eV; $E_{LUMO} = -(E_{onset\ red\ \ Fc/Fc+} + 5.39)$ eV.[27]

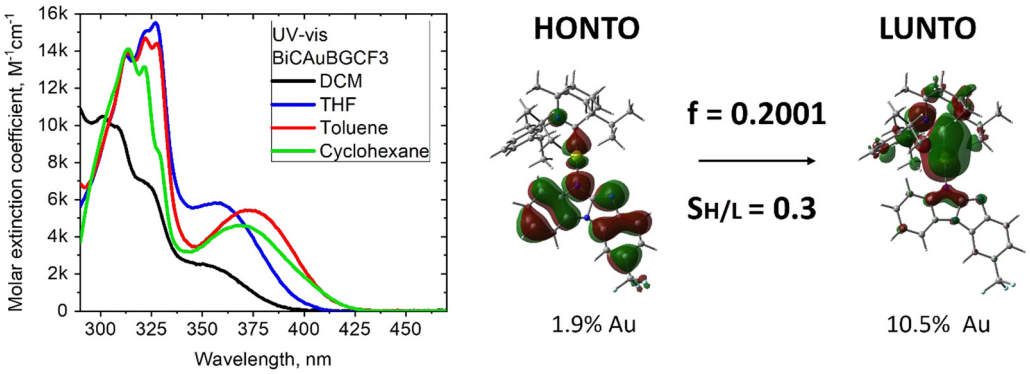

Fig. 3 UV-vis spectra for the **BICAuBGCF3** complex in various solvents at 295 K and pertinent frontier orbitals involved in the lowest energy absorption band.

the range from 300 to 345 nm, ascribed to the intraligand π–π* (IL) transitions of the benzoguanidinato and carbene ligands. A broad low-energy band spanning over a wide range from 325 to 425 nm was assigned to a ligand-to-ligand charge transfer L(M)LCT (M = Au) transition from the benzoguanidinato ligand to the carbene ligand. The assignment is consistent with the analogous complex **Au2** (Scheme 1), with the low-energy absorption bands being 25 nm blue-shifted for **BICAuBGCF3**, thereby reflecting the wider energy gap due to the electron-withdrawing nature of the CF_3 substituent and is in agreement with the electrochemistry results. The CT nature of the low-energy absorption band is supported using TD-DFT theoretical calculations, indicating 97% HOMO → LUMO transition (Fig. 3 and Table S1, ESI†), with 1.9% contribution of the gold orbitals to HOMO and 10.5% to LUMO. Increasing the solvent polarity from cyclohexane to dichloromethane results in a 20-nm blue-shift of the L(M)LCT band (Fig. 3), while the IL band shows little influence from solvent polarity. This is characteristic of CMA materials, which tend to show negative solvatochromism for the low-energy CT band.[18b] There is a significant difference between the ground-state dipole moment of the title complex (15.8 D) and that of the unsubstituted complex **Au2** (11.6 D). This is a result of the CF_3 electron withdrawing group polarizing the amide donor ligand. The dipole moment for the first singlet excited state for **BICAuBGCF3** having an opposite direction is higher (−3.5 D) (Table S2, ESI†) than that for the **Au2** complex (−6.0 D).[25a] The increase in the transition dipole moment of the **BICAuBGCF3** complex agrees with its higher oscillator strength coefficient (0.2001) (*f*, Table S4, ESI† and Fig. 3) compared with **Au2** (0.1897). This can be explained by *f* being directly proportional to the squared value of the transition dipole moment ($|\mu_{S1\rightarrow S0}|^2$).[28]

Photoluminescence properties of the **BICAuBGCF3** complex are presented in Fig. 4, and the data collected together with the analogous unsubstituted complex **Au2** are presented in Table 2. The complex emits deep-blue light at 432 nm when doped in polystyrene (PS) matrices at 1 wt% doping concentration (Fig. 4). The emission profile is broad and unstructured, indicating that the emission originates from a CT excited state. The emission profile is 34 nm blue-shifted from λ_{max} at 466 nm for **Au2**. This fact is in line with the 0.15 eV larger band gap for **BICAuBGCF3**, as measured *via* electrochemistry and UV-vis and predicted through theoretical calculations, *vide infra*. The PLQY of **BICAuBGCF3** is 60%, which is lower than 92% for the analogous **Au2** complex. At 295 K, the **BICAuBGCF3** complex shows a remarkably short sub-microsecond excited state lifetime (τ) with a monoexponential decay of 423 ns, which is similar to that for **Au2** (406 ns). Therefore, the title complex possesses a high radiative rate of up to 1.4×10^6 s^{-1} in amorphous PS films.

In toluene, the **BICAuBGCF3** complex emits a blue light at 478 nm, which is 34 nm blue-shifted compared with **Au2**. However, the solution PLQY value drops to 43% for the title complex, while it drops to near unity for **Au2**. This is likely associated with the dynamic behaviour in the solution

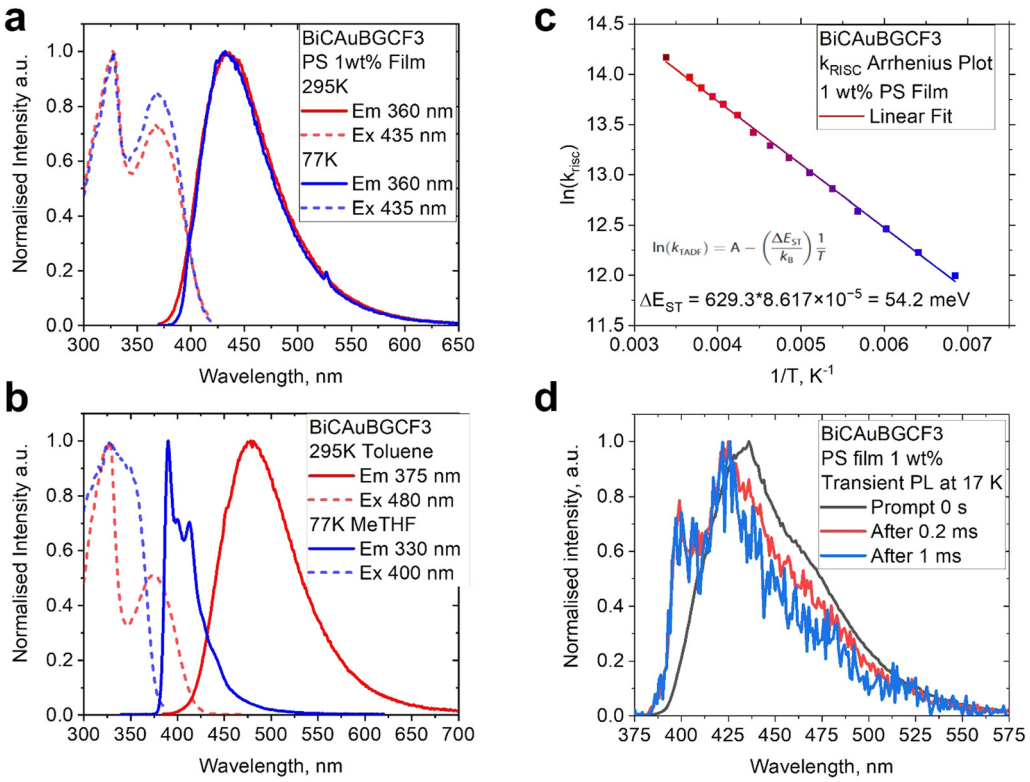

Fig. 4 Excitation and emission spectra for the gold complex **BICAuBGCF3** at 298 and 77 K in 1 wt% polystyrene (PS) films (a), toluene solution and frozen MeTHF glass (b); Arrhenius plot to estimate ΔE_{ST} (c); prompt and delayed (after 0.2 and 1 ms) luminescence profiles at 17 K for the 1 wt% PS film (d).

Table 2 Photophysical properties of the **BiCAuBGCF3** and analogous unsubstituted **Au2** complexes in various matrices

	λ_{em} (nm)	τ (ns)	Φ (%)[a]	k_r (10^6 s^{-1})[b]	k_{nr} (10^5 s^{-1})[c]	CT/LE (eV)[d]	λ_{em} (nm, 77 K)	τ (μs, 77 K)
Toluene solution						MeTHF frozen solution		
Au2	511	493	100	2.03	—	2.77/3.29	414	26.5 (95.16%) 239 (4.84%)
BiCAuBGCF3	478	240	43	1.79	23.8	3.01/3.25	390	150 (9.81%) 625 (45.16%) 1960 (45.03%)
1 wt% PS film								
Au2	466	406	92	2.27	1.97	2.99/—	456	23.5 (46.2%) 41.2 (53.8%)
BiCAuBGCF3	432	423	60	1.42	9.46	3.17/3.23	432	23.9 (90.2%) 258 (9.8%)

[a] Quantum yields determined using an integrating sphere. [b] Radiative rate constant (k_r) = Φ/τ. [c] Nonradiative constant (k_{nr}) = $(1 - \Phi)/\tau$. In case of two-component lifetime (τ), an average was used: $\tau_{av} = (B_1/(B_1 + B_2))\tau_1 + (B_2/(B_1 + B_2))\tau_2$, where B_1 and B_2 are the relative amplitudes for τ_1 and τ_2, respectively. [d] CT/LE energies based on the onset values of the emission spectra blue edge at 77 K.

compared with in the solid state, *vide supra*. The lower PLQY values and shorter emissive lifetime in toluene at 240 ns result in a dominating non-radiative decay rate of 2.38×10^6 s^{-1}, thus indicating energy losses for the title complex in the fluid media.

Theoretical calculations confirm the first CT nature for the S_1 state and the large energy difference of 0.82 eV to the second CT singlet S_2 state (Table S4, ESI†). This significant energy separation validates our focus on the S_1 state for understanding the photophysical behaviour of the title complex, which is in a good agreement with the experimental observations.[29] We previously established that faster TADF is observed for CMA complexes with a locally excited triplet (^{3}LE) state being significantly higher in energy than the CT state.[25a] This inhibits the parasitic, long-lived phosphoresce contribution from the ^{3}LE state. At 77 K in MeTHF, the emission profile becomes highly vibronically resolved with an emissive lifetime in the millisecond regime at 1.18 ms (Table 2). This vibronically resolved profile is ascribed to the phosphorescence from the higher-lying ^{3}LE state. TDDFT calculations demonstrate that ^{3}LE state is localised on the BGCF3 ligand and originates from the HOMO → LUMO+3 (59%) and HOMO → LUMO+4 (20%) transitions. High-energy onsets at 298 K in toluene and frozen

MeTHF glass at 77 K revealed an energy of 3.01 eV for CT and 3.25 eV for ^{3}LE states with an energy difference of 0.24 eV for ΔE(CT–^{3}LE). This is lower than the ΔE(CT–^{3}LE) for the **Au2** complex (0.52 eV); however, it is well above the CT manifold by 0.2 eV. The high energy of the ^{3}LE state of the benzoguanidinato derivative, despite having electron withdrawing CF_3 substituents, allows the occurrence of efficient and fast TADF. This work demonstrates that electron-withdrawing substituents on the benzoguanidinato ligand core are an excellent strategy for tuning the luminescence of TADF CMA emitters to afford deep-blue emission. However, symmetric ligands should be used to avoid isomerism, which can likely lead to reduced PLQY values for the title complex compared with the **Au2** compound.

Another prerequisite for highly efficient CMA TADF is a small exchange energy between the singlet and triplet excited states (ΔE_{ST}). We previously reported that the **Au2** complex exhibits a very small reverse intersystem crossing (rISC) activation energy (ΔE_a) value of 56 meV. Herein, variable-temperature lifetime measurements were conducted to investigate the ΔE_a for the title complex **BiCAuBGCF3**. Upon cooling, the PL profile remains broad and unstructured (Fig. 4), while the emissive lifetime increases to the microsecond regime up to 46.8 μs, which is 100-fold longer compared with the room temperature value (Table 2). The ΔE_a for **BiCAuBGCF3** was estimated using an Arrhenius plot at varied temperatures with $\ln k_{RISC}$ *vs.* $1/T$ to afford 54 meV, which is comparable with 56 meV for the **Au2** complex, thus supporting the rapid radiative rate of TADF. Overall, the title complex possesses the required fast and deep-blue TADF luminescence regardless of the fact that it exists as a mixture of two isomers in fluid media. We were unable to isolate and characterize the isomer **B** for the **BiCAuBGCF3** complex in the solid state; however, our theoretical calculations predict a very similar photoluminescence behavior compared with the isolated isomer **A** (Tables S1–S5, ESI†).

The PS film of the **BiCAuBGCF3** complex exhibited a broad CT luminescence profile (Fig. 4d, black profile) even at 17 K, while the transient photoluminescence experiment revealed the presence of ^{3}LE states (Fig. 4d, red profile after a delay of 0.2 ms) with a clear vibronic structure. This experiment enabled us to determine that the energy gap ΔE(CT–^{3}LE) is −0.06 eV in the PS film, which is considerably smaller compared with that in the fluid media (−0.24 eV) (Table 2, see MeTHF data). Such a large difference reflects a highly polar nature of the CMA material, *i.e.* lower the polarity of the media, greater the destabilization of the CT state (blue-shift in luminescence).

Conclusion

We prepared and fully characterised a gold(I)-based CMA complex with BiCAAC-carbene and a novel benzoguanide ligand having electron-withdrawing CF_3 substituent. The asymmetric substitution of the ligand affords two possible isomers of the gold CMA material **BICAuBGCF3** complex, which were observed using ^{1}H and ^{13}F NMR spectroscopy. In the solid state, the complex exists in a form where (carbene)gold(I) and CF3 moieties are located on the opposite sites of the benzindole ring of the ligand **L**. Such a CF3-substituted BG-CMA material possesses a stabilised HOMO energy level shifted by 0.27 eV, leading to a wider HOMO–LUMO gap and deep-blue emission compared with the unsubstituted BG-CMA material. This isomerism leads to reduced quantum yields (43%) and a pronounced non-radiative decay process with a rate of up to 2×10^{-6} s^{-1} in fluid media. The title complex avoids parasitic phosphorescence from the amide-based ^{3}LE state, demonstrating that electron-withdrawing substitution at the benzoguanidinato amide ligand is a good strategy for achieving optimal deep-blue thermally activated delayed fluorescence at 432 nm in polystyrene films. The **BICAuBGCF3** complex possesses bright PLQY values of up to 60% with rapid radiative rates of up to 1.42×10^{-6} s^{-1}. Future studies should use symmetric benzoguanidinato ligands to improve PLQY values up to unity by reducing non-radiative pathways to prevent dynamic isomerism processes.

Author contributions

A. B. performed the synthesis, steady-state photoluminescence and electrochemistry studies. A. S. R. performed X-ray crystallography. N. L. P. and M. L. carried out theoretical calculations and data analysis. A. S. R. and M. L. planned the project and designed the experiments. A. B. and A. S. R. co-wrote the manuscript. All the authors contributed to the discussion of the results, analysis of the data and review of the manuscript.

Conflicts of interest

The authors declare no competing interests.

Data availability

The data supporting this article have been included as part of the ESI.†

Acknowledgements

A. S. R. acknowledges the support from the Royal Society (grant no. URF\R1\180288, RGF\EA\181008, and URF\R\231014) and the EPSRC (grant code EP/K039547/1 and APP46952). M. L. acknowledges the Academy of Finland Flagship Programme, Photonics Research and Innovation (PREIN), decision 320166, the Finnish Grid and Cloud Infrastructure resources (urn:nbn:fi:research-infras-2016072533). N. L. P. acknowledges the Doctoral Programme in Science, Forestry and Technology (Lumeto, University of Eastern Finland). We thank Dr Louise Natrajan, EPSRC, and University of Manchester for access to the Centre for Radiochemistry Research National Nuclear User's Facility (NNUF, EP/T011289/1) to use the FLS-1000 fluorometer.

References

1 G. Hong, X. Gan, C. Leonhardt, Z. Zhang, J. Seibert, J. M. Busch and S. Bräse, A Brief History of OLEDs-Emitter Development and Industry Milestones, *Adv. Mater.*, 2021, **33**(9), e2005630.

2 S. Castelletto and A. Boretti, Luminescence solar concentrators: A technology update, *Nano Energy*, 2023, **109**, 108269.

3 E. H. Onah, N. L. Lethole and P. Mukumba, Luminescent Materials for Dye-Sensitized Solar Cells: Advances and Directions, *Appl. Sci.*, 2024, **14**(20), 9202.

4 H. Uoyama, K. Goushi, K. Shizu, H. Nomura and C. Adachi, Highly efficient organic light-emitting diodes from delayed fluorescence, *Nature*, 2012, **492**, 234–238.

5 A. Arjona-Esteban and D. Volz, Status and Next Steps of TADF Technology: An Industrial Perspective, *Highly Effic. OLEDs*, 2018, 543–572.

6 C.-Y. Chan, L.-S. Cui, J. U. Kim, H. Nakanotani and C. Adachi, Rational Molecular Design for Deep-Blue Thermally Activated Delayed Fluorescence Emitters, *Adv. Funct. Mater.*, 2018, **28**(11), 1706023.

7 J. Eng and T. J. Penfold, Understanding and Designing Thermally Activated Delayed Fluorescence Emitters: Beyond the Energy Gap Approximation, *Chem. Rec.*, 2020, **20**(8), 831–856.

8 V. Ferraro, C. Bizzarri and S. Bräse, Thermally Activated Delayed Fluorescence (TADF) Materials Based on Earth-Abundant Transition Metal Complexes: Synthesis, Design and Applications, *Adv. Sci.*, 2024, **11**(34), 2404866.

9 J. M. Dos Santos, D. Hall, B. Basumatary, M. Bryden, D. Chen, P. Choudhary, T. Comerford, E. Crovini, A. Danos and J. De, *et al.*, The Golden Age of Thermally Activated Delayed Fluorescence Materials: Design and Exploitation, *Chem. Rev.*, 2024, **124**(24), 13736–14110.

10 D. Di, A. S. Romanov, L. Yang, J. M. Richter, J. P. Rivett, S. Jones, T. H. Thomas, M. Abdi Jalebi, R. H. Friend and M. Linnolahti, *et al.*, High-performance light-emitting diodes based on carbene–metal–amides, *Science*, 2017, **356**, 159–163.

11 M. Gernert, L. Balles-Wolf, F. Kerner, U. Müller, A. Schmiedel, M. Holzapfel, C. M. Marian, J. Pflaum, C. Lambert and A. Steffen, Cyclic (Amino)(aryl)carbenes Enter the Field of Chromophore Ligands: Expanded π System Leads to Unusually Deep Red Emitting CuI Compounds, *J. Am. Chem. Soc.*, 2020, **142**(19), 8897–8909.

12 A. Ying and S. Gong, A Rising Star: Luminescent carbene–metal–amides Complexes, *Chem. – Eur. J.*, 2023, **29**(59), e202301885.

13 A. S. Romanov, S. T. E. Jones, Q. Gu, P. J. Conaghan, B. H. Drummond, J. Feng, F. Chotard, L. Buizza, M. Foley and M. Linnolahti, *et al.*, Carbene metal amide photoemitters: tailoring conformationally flexible amides for full color range emissions including white-emitting OLED, *Chem. Sci.*, 2020, **11**(2), 435–446.

14 A. Ruduss, B. Turovska, S. Belyakov, K. A. Stucere, A. Vembris, G. Baryshnikov, H. Ågren, J.-C. Lu, W.-H. Lin, C.-H. Chang and K. Traskovskis, Thiazoline Carbene–Cu(I)–Amide complexes: Efficient White Electroluminescence from Combined Monomer and Excimer Emission, *ACS Appl. Mater. Interfaces*, 2022, **14**(13), 15478–15493.

15 R. Tang, S. Xu, L. Du, F.-F. Hung, T.-L. Lam, G. Cheng, K.-H. Low, Q. Wan, S. Wu, Y. Chen and C.-M. Che, Au(I)-TADF Emitters for High Efficiency Full-ColorVacuum-Deposited OLEDs and TADF-SensitizedFluorescent OLEDs with Ultrahigh Brightness and Prolonged Operational Lifetime, *Adv. Opt. Mater.*, 2023, **11**, 2300950.

16 L. Zhan, A. Ying, Y. Qi, K. Wu, Y. Tang, Y. Tan, Y. Zou, G. Xie, S. Gong and C. Yang, Copper(I) Complex as Sensitizer Enables High-Performance Organic Light-Emitting Diodes with Very Low Efficiency Roll-Off, *Adv. Funct. Mater.*, 2021, **31**, 2106345.

17 Q. Gu, F. Chotard, J. Eng, A. M. Reponen, I. J. Vitorica-Yrezabal, A. W. Woodward, T. J. Penfold, D. Credgington, M. Bochmann and A. S. Romanov, Excited-State Lifetime Modulation by Twisted and Tilted Molecular Design in carbene–metal–amides Photoemitters, *Chem. Mater.*, 2022, **34**(16), 7526–7542.

18 (*a*) A. S. Romanov, S. T. E. Jones, L. Yang, P. J. Conaghan, D. Di, M. Linnolahti and D. Credgington, M. Bochmann. Mononuclear Silver Complexes for Efficient Solution and Vacuum-Processed OLEDs, *Adv. Opt. Mater.*, 2018, 1801347; (*b*) J. Feng, A.-P. M. Reponen, A. S. Romanov, M. Linnolahti, M. Bochmann, N. C. Greenham, T. Penfold and D. Credgington, Influence of Heavy Atom Effect on the Photophysics of Coinage Metal carbene–metal–amides Emitters. Adv, *Funct. Mater.*, 2021, **31**(1), 2005438; (*c*) R. Hamze, S. Shi, S. C. Kapper, D. S. Muthiah Ravinson, L. Estergreen, M.-C. Jung, A. C. Tadle, R. Haiges, P. I. Djurovich and J. L. Peltier, *et al.*, "Quick-Silver" from a Systematic Study of Highly Luminescent, Two-Coordinate, d10 Coinage Metal Complexes, *J. Am. Chem. Soc.*, 2019, **141**(21), 8616–8626.

19 C. N. Muniz, J. Schaab, A. Razgoniaev, P. I. Djurovich and M. E. Thompson, π-Extended Ligands in Two-Coordinate Coinage Metal Complexes, *J. Am. Chem. Soc.*, 2022, **144**(39), 17916–17928.

20 P. J. Conaghan, C. S. B. Matthews, F. Chotard, S. T. E. Jones, N. C. Greenham, M. Bochmann, D. Credgington and A. S. Romanov, Highly efficient blue organic light-emitting diodes based on carbene–metal–amidess, *Nat. Commun.*, 2020, **11**(1), 1758.

21 J. Feng, E. J. Taffet, A.-P. M. Reponen, A. S. Romanov, Y. Olivier, V. Lemaur, L. Yang, M. Linnolahti, M. Bochmann, D. Beljonne and D. Credgington, Carbene–Metal–Amide Polycrystalline Materials Feature Blue Shifted Energy yet Unchanged Kinetics of Emission, *Chem. Mater.*, 2020, **32**(11), 4743–4753.

22 R. Li, A. Ying, Y. Tan, Y. Ai and S. Gong, Efficient Blue Photo- and Electroluminescence from CF3-Decorated Cu(I) Complexes, *Chem. – Eur. J.*, 2024, **30**, e202400817.

23 Q. Gu, S. Gorgon, A. S. Romanov, F. Li, R. H. Friend and E. Evans, Fast Transfer of Triplet to Doublet Excitons from Organometallic Host to Organic Radical Semiconductors, *Adv. Mater.*, 2024, 2402790.

24 A.-P. M. Reponen, F. Chotard, A. Lempelto, V. Shekhovtsev, D. Credgington, M. Bochmann, M. Linnolahti, N. C. Greenham and A. S. Romanov, Donor N-Substitution as Design Principle for Fast and Blue Luminescence in carbene–metal–amidess, *Adv. Opt. Mater.*, 2022, **10**(15), 2200312.

25 (*a*) A. C. Brannan, H.-H. Cho, A.-P. M. Reponen, S. Gorgon, N. L. Phuoc, M. Linnolahti, N. C. Greenham and A. S. Romanov, Deep-Blue and Fast Delayed Fluorescence from Carbene–Metal–Amides for Highly Efficient and Stable Organic Light-Emitting Diodes, *Adv. Mater.*, 2024, **36**(30), 2404357; (*b*) C. Riley, H.-H. Cho, A. Brannan, N. L. Phuoc, M. Linnolahti, N. Greenham and A. S. Romanov, High Triplet Energy Host Material with a 1, 3, 5-Oxadiazine Core from a One-step Interrupted Fischer Indolization, *Commun. Chem.*, 2024, **7**, 298.

26 A. S. Romanov, F. Chotard, J. Rashid and M. Bochmann, Synthesis of copper(I) cyclic (alkyl)(amino)carbene complexes with potentially bidentate N,N and S,S ligands for efficient white photoluminescence, *Dalton Trans.*, 2019, **48**, 15445–15454.

27 C. M. Cardona, W. Li, A. E. Kaifer, D. Stockdale and G. C. Bazan, Electrochemical considerations for determining absolute frontier orbital energy levels of conjugated polymers for solar cell applications, *Adv. Mater.*, 2011, **23**(20), 2367–2371.

28 A. W. Kanzler, H. Sun and K. F. Freed, Dipole moments, transition moments, oscillator strengths, radiative lifetimes, and overtone intensities for CH and CH+ as computed by quasi-degenerate many-body perturbation theory, *Int. J. Quantum Chem.*, 1991, **39**, 269–286.

29 Note, the multireference configuration interaction (MRCI) method has been demonstrated to provide a more accurate description of the excited states and validated against spectroscopical data for various materials including CMA complexes, see (*a*) J. Föller and C. M. Marian, Rotationally Assisted Spin-State Inversion in carbene–metal–amides Is an Artifact, *J. Phys. Chem. Lett.*, 2017, **8**, 5643–5647; (*b*) T. J. Penfold, E. Gindensperger, C. Daniel and C. M. Marian, Spin-Vibronic Mechanism for Intersystem Crossing, *Chem. Rev.*, 2018, **118**(15), 6975–7025; (*c*) S. Thompson, J. Eng and T. J. Penfold, The Intersystem Crossing of a Cyclic (alkyl)(amino) carbene gold (I) complex, *J. Chem. Phys.*, 2018, **149**, 0143304; (*d*) C. M. Marian, A. Heil and M. Kleinschmidt, The DFT/MRCI method, *WIREs Comput. Mol. Sci.*, 2019, **9**, e1394; (*e*) A. Heil, M. Kleinschmidt and C. M. Marian, On the performance of DFT/MRCI Hamiltonians for electronic excitations in transition metal complexes: The role of the damping function, *J. Chem. Phys.*, 2018, **149**, 164106; (*f*) A. Liske, L. Wallbaum, T. Hölzel, J. Föller, M. Gernert, B. Hupp, C. Ganter, C. M. Marian and A. Steffen, Cu–F Interactions between Cationic Linear N-Heterocyclic Carbene Copper(I) Pyridine Complexes and Their Counterions Greatly Enhance Blue Luminescence Efficiency, *Inorg. Chem.*, 2019, **58**(9), 5433–5445; (*g*) J. Eng, S. Thompson, H. Goodwin, D. Credgington and T. J. Penfold, Competition between the heavy atom effect and vibronic coupling in donor–bridge–acceptor organometallics, *Phys. Chem. Chem. Phys.*, 2020, **22**, 4659–4667.